Minimal Coordinate Formulation of Contact Dynamics in Operational Space

Abhinandan Jain, Cory Crean, Calvin Ku, Steven Myint
Jet Propulsion Laboratory, California Institute of Technology
Pasadena, CA 91109

Hubertus von Bremen
California State Polytechnic University
Pomona, CA 91768

***Abstract*—In recent years, complementarity techniques have been developed for modeling non-smooth contact and collision dynamics problems for multi-link robotic systems. Normally, in this approach, a linear complementarity problem (LCP) is set up using $6n$ non-minimal coordinates for a system with n links together with all the unilateral constraints and inter-link bilateral constraints on the system. In this paper, we use operational space dynamics to develop a complementarity formulation for contact and collision dynamics that uses *minimal* coordinates. The use of such non-redundant coordinates results in much smaller size LCP problems and the automatic enforcement of the inter-link bilateral constraints. Furthermore, we exploit operational space low-order computational algorithms to overcome some of the bottlenecks in using minimal coordinates.**

I. Introduction

For more than a decade, researchers [1, 9, 11] have been developing complementarity based approaches to formulating and solving the dynamics of systems with contact and collision dynamics. Examples of such dynamics for robotic systems include manipulation and grasping tasks and legged locomotion. This approach models bodies as rigid, and uses impulsive dynamics to handle non-smooth collision, contact interactions and state transitions. By essentially impulsively "stepping" over non-smooth events, complementarity methods avoid the the small step size and stiff dynamics problems encountered with penalty based methods which model surface deformation dynamics during contact [7].

The complementarity approach involves setting up of a *linear complementarity problem (LCP)* that depends on the link mass and inertia properties, contact friction parameters, inter-link bilateral constraints and the contact and collision unilateral constraints [1, 9, 11]. The LCP solution identifies the unilateral constraints that are active, and solves for the impulsive forces and velocity changes that are consistent with the constraints on the system. Variants of the complementarity approach to handle elastic collisions have also been developed [1]. While the standard LCP formulation uses a discretized approximation for the friction cones, other researchers [10] have explored non-linear cone complementarity approaches that avoid such approximations.

For a multi-link system with n links, the normal approach to set up the associated LCP problem uses $6n$ non-minimal coordinates [11] together with the bilateral constraints associated with the inter-link hinges and the unilateral contact constraints. This approach has a simpler system mass matrix that is block diagonal and constant. On the other hand, such redundant coordinates lead to large LCP problem size, and require the use of differential-algebraic equation (DAE) like techniques for managing error drift in the bilateral constraints when integrating the equations of motion.

An alternative approach uses minimal hinge coordinates that automatically eliminate the bilateral constraints for the inter-link hinges [12]. While the underlying physics remains unchanged, this formulation reduces the size of the LCP problems, and avoids the need for DAE techniques for controlling bilateral constraint violation errors for the inter-link hinges. However, the use of minimal coordinate leads to a dense and configuration dependent mass matrix. This makes the LCP problem setup more complicated, and has been a significant hurdle in the use of such a minimal coordinate approach.

In this paper, we focus on the analytical and computational aspects of the minimal coordinate formulation of the complementarity approach to contact and collision dynamics for multi-link systems. We adopt the complementarity based physics models from [1, 11], but reformulate the system dynamics and the associated LCP problem using minimal coordinates. While [12] used a similar minimal coordinate formulation, it was limited to just contact dynamics, and used the divide-and-conquor (DCA) technique [2] as part of its solution technique. This paper goes beyond contact dynamics to also develop the LCP variants for handling elastic and inelastic collision dynamics. Moreover, for closed-chain topology systems, we describe a uniform way to incorporate the bilateral constraint associated with the closure constraint naturally into the LCP problem. Our minimal coordinates approach adopts an *operational space* [5] perspective, which in turn allows us to take advantage of low-order spatial operator algorithms [3, 4, 6] for computing the *operational space complementarity matrix (OSCM)* sub-matrices needed for setting up the LCP problem. Taken together the methods described here provide a comprehensive, and computationally tractable, solution to using minimal coordinates for contact and collision dynamics problems. We conclude with results from an illustrative multi-link pendulum numerical problem.

II. Equations of Motion

A. Minimal coordinate dynamics

The minimal coordinate equations of motion for a tree-topology multi-link robotic system with n links and N degrees

of freedom take the form

$$T = M\ddot{\theta} + C - J^{*}f_c \tag{1}$$

where $\theta \in R^N$ denotes the generalized coordinates, $T \in R^N$ the generalized forces, $M \in R^{N\times N}$ the system mass matrix, $C \in R^N$ the vector of Coriolis, gyroscopic and gravitational forces, $f_c \in R^{6n_c}$ the stacked vector of nodal forces for n_c nodes on the system, and $J \in R^{6n_c\times N}$ the Jacobian matrix for these nodes.

While the values of the f_c nodal force components that arise from control actuators may be known, the ones associated with system constraints are not explicitly available. In this paper, we will assume that f_c only contains such implicit constraint forces, since the effect of the explicit ones is easily handled by absorbing them into the C term. In view of this, all nodes in this paper will refer to constraint nodes.

In a minimal coordinates formulation, bilateral constraints associated with inter-link hinges are eliminated by using hinge coordinates that directly parameterize the hinge motion. Thus tree-topology systems have no bilateral constraints for such models. Bilateral constraints on the other hand are unavoidable for closed-chain topology systems. Such systems are decomposed into a tree-topology system (from a spanning tree) together with a minimal set of bilateral closure constraints. Thus Eq. 1 will always refer to the equations of motion for the tree-topology part of the system, the closure constraints will define the bilateral constraints, while the contact constraints will form the set of unilateral constraints on the system.

The $\ddot{\theta}$ generalized solution of Eq. 1 can be expressed as

$$\ddot{\theta} = M^{-1}J^{*}f_c + \ddot{\theta}_f \text{ where } \ddot{\theta}_f \triangleq M^{-1}(T - C) \tag{2}$$

$\ddot{\theta}_f$ represents the *free* generalized accelerations, i.e. the generalized accelerations in the absence of the nodal forces. Eq. 2 expresses the overall $\ddot{\theta}$ generalized acceleration for the system as the sum of the $\ddot{\theta}_f$ free generalized accelerations and the $M^{-1}J^{*}f_c$ correction acceleration contribution from the implicit non-zero nodal forces. The following section describes the *operational space* form of the equations of motion that describe the mapping between the nodal forces to the nodal spatial accelerations.

B. Operational space dynamics

The operational space for our multi-link system is defined instantaneously by the configuration of the set of constraint nodes on the system. $V_c \in R^{6n_c}$ denotes the stacked vector of spatial velocities [?] of all the n_c nodes. The relationship between V_c and the $\dot{\theta}$ joint velocities is given by

$$V_c = J\dot{\theta} \tag{3}$$

The task space spatial acceleration $\alpha_c \in R^{6n_c}$ is defined as the time derivative of V_c and, from Eq. 3, its expression is

$$\alpha_c \triangleq \frac{dV_c}{dt} \overset{3}{=} J\ddot{\theta} + a_{os} \quad \text{where} \quad a_{os} \triangleq \dot{J}\dot{\theta} \tag{4}$$

Denoting the node accelerations for the free system (i.e. without the f_c nodal forces) by α_f, the following analog of Eq. 4 defines α_f in terms of the $\ddot{\theta}_f$ generalized accelerations:

$$\alpha_f \triangleq J\ddot{\theta}_f + a_{os} \tag{5}$$

Pre-multiplying Eq. 2 by J and using Eq. 4 yields:

$$\alpha_c \overset{4,5,2}{=} \bar{\Lambda} f_c + \alpha_f \text{ where } \bar{\Lambda} \triangleq JM^{-1}J^{*} \in R^{6n_c\times 6n_c} \tag{6}$$

$\bar{\Lambda}$ is referred to as the *operational space compliance matrix (OSCM)*. The invertibility of $\bar{\Lambda}$ does not depend on J being invertible – only that J have full row-rank. When it exists, the inverse of $\bar{\Lambda}$ is referred to as the operational space inertia.

C. Impulsive dynamics

The differential form of equations of motion in Eq. 2 can be discretized using an Euler setp to obtain a form that maps a p impulse stacked vector at the nodes into the resulting change in generalized or nodal spatial velocities over a Δ_t time interval[1]

$$\frac{\dot{\theta}^{+} - \dot{\theta}^{-}}{2} = M^{-1}J^{*}p + \ddot{\theta}_f\Delta_t \text{ with } p \triangleq f_c\Delta_t \tag{7}$$

Multiplying both sides with J leads to

$$V_c^{+} - V_c^{-} \overset{3,7}{=} \bar{\Lambda}p + \alpha_f\Delta_t \tag{8}$$

Collision events are impulsive and lead to instantaneous changes in the system velocities, and in this case $\Delta_t = 0$ in the above equations.

III. Unilateral contact constraints

Unilateral constraints are defined by inequality relationships such as:

$$d(\theta, t) \geq 0 \tag{9}$$

As an example, the non-penetration condition for rigid bodies can be stated as an inequality relationship requiring that the distance between the surfaces of rigid bodies be non-negative. $d(\theta, t)$ is generally referred to as the *distance* or *gap* function for unilateral constraints.

Contact occurs at the constraint boundary, i.e., when $d(\theta, t) = 0$. For bodies in contact, the surface normals at the contact point are parallel. The existence of contact is often determined using geometric or collision detection techniques. For a pair of bodies A and B in contact, we use a convention where the ith contact normal $\hat{n}(i)$ is defined as pointing from body B towards body A, so that motion of A in the direction of the normal will lead to separation of the bodies [2].

A unilateral constraint is said to be in an *active* state when

$$d(\theta, t) = \dot{d}(\theta, t) = \ddot{d}(\theta, t) = 0 \tag{10}$$

Thus, a unilateral constraint is active when there is contact, and the contact persists. Only active constraints generate constraint forces on the system.

[1] The $-$ and $+$ superscripts will denote the respective value of a quantity just before and after the application of an impulse.

[2] This is the same convention for contact normals as used by the *Bullet* physics engine.

A constraint that is not active is said to be *inactive*. Contact *separation* occurs when the relative linear velocity of the contact points along the normals becomes positive and the contact points drift apart. A separating constraint is in the process of losing contact and transitioning to an inactive state. At the start of a separation event, we have

$$d(\theta, t) = \dot{d}(\theta, t) = \mathbf{0} \quad \text{and} \quad \ddot{d}(\theta, t) > \mathbf{0} \tag{11}$$

A. Contact impulse for an active contact constraint

We now describe contact force models based upon the approach in references [1, 11]. Denote the number of unilateral contact nodes by n_u. The 6-dimensional spatial impulse at the ith active contact constraint node has a zero angular moment component. Its non-zero linear impulse component $F_u(i) \in R^3$ can be decomposed into normal and tangential (friction impulse) components

$$F_u(i) = F_n(i)\hat{n}(i) + F_t(i)\hat{t}(i) \tag{12}$$

Assuming that the friction coefficient is $\mu(i)$, the magnitude of the tangential Coulombic frictional impulse is bounded by the magnitude of the normal component as follows:

$$|F_t(i)| \le \mu(i)F_n(i) \tag{13}$$

When the relative linear velocity between the contact nodes is non-zero, the tangential frictional impulse is in a direction opposite to the linear velocity vector (which necessarily lies in the contact tangent plane) and Eq. 13 holds with an equality. When the bodies have non-zero relative velocities at the contact point, the contact is said to be a **sliding** contact. Otherwise, when the relative linear velocity is zero, the contact is said to be a **rolling** contact. Thus, the tangential friction impulse is on the boundary of the cone defined by Eq. 13 when sliding, and in the interior of the cone when rolling.

For the purpose of numerical computation, the friction cone is approximated by a friction polyhedron consisting of a finite number, n_f, of unit direction vectors $\hat{d}_j(i)$ in the tangent plane. It is assumed that for each direction vector, its opposite direction vector is also in the set. For notational simplicity, we assume that n_f is the same across all contact points. The tangential frictional impulse is expressed as the linear combination of these direction vectors as follows:

$$\begin{aligned} F_t(i)\hat{t}(i) &= \sum_{j=0}^{n_f} \beta_j(i)\hat{d}_j(i) = D(i)\beta(i) \\ \text{where } D(i) &\triangleq \left[\hat{d}_1(i), \cdots, \hat{d}_{n_f}(i)\right] \in R^{3 \times n_f} \\ \text{and } \beta(i) &= \mathrm{col}\{\beta_j(i)\}_{j=1}^{n_f} \in R^{n_f} \end{aligned} \tag{14}$$

Combining together Eq. 12 and Eq. 14, we have

$$\begin{aligned} F_u(i) = \underline{D}(i)\underline{\beta}(i) \text{ where } \underline{\beta}(i) &\triangleq \begin{bmatrix} F_n(i) \\ \beta(i) \end{bmatrix} \in R^{n_f+1} \\ \text{and } \underline{D}(i) &\triangleq \left[\hat{n}(i),\ D(i)\right] \in R^{3 \times (n_f+1)} \end{aligned} \tag{15}$$

During sliding, $\beta_j(i)$ is non-zero and equal to $\mu(i)F_n(i)$ for just the single j that corresponds to the closest direction opposing the relative linear velocity. In other words, with $\sigma(i)$ denoting the magnitude of the contact relative velocity,

$$\beta_k(i) = \begin{cases} \mu(i)F_n(i)\,1_{[k=j]} & \text{if } \sigma(i) > 0 \\ 0 & \text{if } \sigma(i) = 0 \end{cases} \tag{16}$$

In the above, $1_{[\langle cond \rangle]}$ denotes the indicator function whose value is 1 if the condition is true, and 0 otherwise.

B. Complementarity relationship for a unilateral contact

The sliding/rolling contact relationships can be stated equivalently as the following complementarity[3] conditions:

$$\begin{aligned} \hat{n}^*(i)v_u^+(i) &\perp F_n(i) && \text{(separation)} \\ \sigma(i)E(i) + D^*(i)v^+(i) &\perp \beta(i) && \text{(friction force direction)} \\ \mu(i)F_n(i) - E^*(i)\beta(i) &\perp \sigma(i) && \text{(friction force magnitude)} \end{aligned} \tag{17}$$

$$\text{where} \quad E(i) = \mathrm{col}\{1\}_{j=1}^{n_f} \in R^{n_f} \tag{18}$$

and $v_u^+(i) \in R^3$ denotes the linear relative velocity of the first body A with respect to the second body B. The component of this relative velocity along the contact normal is, $\hat{n}^*(i)v_u^+(i)$, and a positive value indicates increasing separation between the bodies, while a negative value indicates that the bodies are approaching each other. The complementarity conditions in Eq. 17 enforce the no inter-penetration constraint at the velocity level, instead of at the gap-level, hence they are really valid only when the gap is zero, i.e., when contact exists [1]. Using Eq. 15, Eq. 17 can be alternatively expressed as

$$\begin{aligned} \hat{E}(i)\sigma(i) + D^*(i)v_u^+(i) &\perp \underline{\beta}(i) \\ \bar{E}(i)\underline{\beta}(i) &\perp \sigma(i) \end{aligned} \tag{19}$$

$$\begin{aligned} \text{where} \quad \hat{E}(i) &\triangleq \begin{bmatrix} 1 \\ 0 \end{bmatrix} \in R^{n_f+1} \\ \text{and} \quad \bar{E}(i) &\triangleq \begin{bmatrix} \mu(i), & -E^*(i) \end{bmatrix} \in R^{1 \times n_f+1} \end{aligned} \tag{20}$$

C. Aggregated complementarity relationships

The stacked vector of relative linear velocities at the contacts is denoted $v_u^+ \in R^{3n_u}$. It can be obtained from the stacked vector of node spatial velocities $V_c^+ \in R^{6n_c}$ via the following relationship

$$v_u = Q_u V_c^+ \tag{21}$$

where the $Q_u \in R^{3n_u \times 6n_c}$ matrix contains one block-row per contact node-pair, with each row mapping the spatial velocities of the node pair into the relative linear velocity across the contact. The motivation for defining and using the Q_u matrix is that it allows us to handle both unilateral constraints in a manner very similar to that for bilateral constraints in the operational space formulation. Q_u has exactly the same structure as the Q_b constraint mapping matrix for bilateral constraints in Eq. 32 for three degree of freedom spherical hinges.

[3] A pair of vectors a and b are said to be complementary, i.e., $a \perp b$ if for each index i, either $a(i)$ or $b(i)$ is zero.

The Q_u matrix is also involved in the dual relationship between the F_u equal and opposite impulse forces at contact node-pairs and the corresponding spatial impulses, p at the individual nodes via

$$p = Q_u^* F_u \in R^{6n_c} \tag{22}$$

Define

$$\underline{\beta} \triangleq \mathrm{col}\{\underline{\beta}(i)\}_{i=0}^{n_u} \in R^{n_u(n_f+1)}$$
$$\text{and} \quad \sigma \triangleq \mathrm{col}\{\sigma(i)\}_{i=0}^{n_u} \in R^{n_u} \tag{23}$$

From Eq. 15, we have

$$F_u \triangleq \mathrm{col}\{F_u(i)\}_{i=1}^{n_u} = \underline{D}\underline{\beta} \in R^{3n_u}$$
$$\text{where} \quad \underline{D} \triangleq \mathrm{diag}\{D(i)\}_{i=1}^{n_u} \in R^{3n_u \times n_u(n_f+1)} \tag{24}$$

Thus,

$$p \overset{22,24}{=} Q_u^* \underline{D}\underline{\beta} \tag{25}$$

Now we examine the effect of the contact node impulses on the node spatial velocities.

$$V_c^+ - V_c^- \overset{8}{=} \bar{\Lambda} p + \Delta_t \alpha_f \overset{24}{=} \Lambda Q_u^* \underline{D}\underline{\beta} + \Delta_t \alpha_f \tag{26}$$

Pre-multiplying Eq. 26 by $\underline{D}^* Q_u$ we obtain

$$\underline{D}^* v_u^+ \overset{21}{=} (\underline{D}^* Q_u \Lambda Q_u^* \underline{D})\underline{\beta} + \Delta_t \underline{D}^* Q_u \alpha_f + \underline{D}^* v_u^- \tag{27}$$

Combining equations 19 and 27, and in the absence of bilateral constraints, the overall complementarity conditions can be rephrased as:

$$\begin{bmatrix} \underline{D}^* Q_u \Lambda Q_u^* \underline{D} & \hat{E} \\ \bar{E} & 0 \end{bmatrix} \begin{bmatrix} \underline{\beta} \\ \sigma \end{bmatrix} + \begin{bmatrix} \underline{D}^*(Q_u \Delta_t \alpha_f + v_u^-) \\ 0 \end{bmatrix} \perp \begin{bmatrix} \underline{\beta} \\ \sigma \end{bmatrix} \tag{28}$$

$$\text{where} \quad \hat{E} \triangleq \mathrm{diag}\{\hat{E}(i)\}_{i=1}^{n_u} \in R^{n_u(n_f+1) \times n_u}$$
$$\bar{E} \triangleq \mathrm{diag}\{\bar{E}(i)\}_{i=1}^{n_u} \in R^{n_u \times n_u(n_f+1)} \tag{29}$$

The structure of the LCP problem in Eq. 28 is different from that normally found in literature [1, 11, 12]. This difference arises from the way we have defined $\underline{\beta}(i)$ in Eq. 15 and used it to arrange the coordinates in the LCP problem. This combined way of organizing the coordinates on a per contact constraint will allow us to handle unilateral and bilateral constraints in a uniform manner. The key take away is that the structural difference is not a reflection of any difference in the underlying physics of the problem. The solution to this $n_u(n_f+2)$ dimensional LCP yields $\underline{\beta}$ and σ and it can be used to propagate the system state as follows:

$$p = Q_u^* \underline{D}\underline{\beta}$$
$$\ddot{\theta} = \ddot{\theta}_f + M^{-1} J^* (p / \Delta_t) \tag{30}$$

The second equation can be numerically integrated until there is a new collision event during the Δ_t propagation interval. Observe that the p contact impulse is averaged over the Δ_t time interval to get the spatial forces at the contact nodes. A simple Euler step integration based discretization of Eq. 30 is:

$$p = Q_u^* \underline{D}\underline{\beta}$$
$$\dot{\theta}^+ = \dot{\theta}^- + M^{-1} J^* p + \Delta_t \ddot{\theta}_f \tag{31}$$

An LCP solution with $F_u(i)$ positive indicates that the ith contact is *active*. Furthermore, a zero $\sigma(i)$ implies that the ith contact is a *rolling contact* while a non-zero value implies that it is a *sliding* contact.

D. Including bilateral constraints

As discussed earlier, in the minimal coordinate formulation, bilateral constraints arise from closure constraints associated with closed-chain topology systems. Tree topology systems have no bilateral closure constraints. We now describe extensions to the previous section's complementarity formulation when the system has non-zero bilateral constraints. From now on, n_u will denot the total number of constraint nodes for the unilateral and bilateral constraints.

Assuming that n_b denotes the size of the bilateral constraints on the system, a bilateral constraint matrix $Q_b \in R^{n_b \times 6n_c}$ can be used to characterize the effect of these constraints as follows:

$$Q_b V_c = 0 \tag{32}$$

Eq. 22 and Eq. 25 for the node impulse generalize to

$$p = Q_u^* F_u + Q_b^* \lambda \overset{24}{=} Q_u^* \underline{D}\underline{\beta} + Q_b^* \lambda \tag{33}$$

where λ denote the Lagrange multipliers associated with the bilateral constraints. p now contains force contributions from the unilateral as well as the bilateral constraints.

To handle the bilateral constraints, $\underline{\Lambda}$ in Eq. 27 expands to be the OSCM for all the unilateral and bilateral constraint nodes. Using Eq. 33 in place of Eq. 25, the generalization of the complementarity condition in Eq. 28 that includes bilateral constraints is as follows:

$$\begin{bmatrix} \underline{D}^* Q_u \Lambda [Q_u^* \underline{D}, Q_b^*] & \hat{E} & 0 \\ \bar{E} & 0 & 0 \\ 0 & 0 & 0 \end{bmatrix} \begin{bmatrix} \underline{\beta} \\ \lambda \\ \sigma \end{bmatrix} + \begin{bmatrix} \underline{D}^* Q_u \Delta_t \alpha_f + \underline{D}^* v_u^- \\ 0 \\ 0 \end{bmatrix} \perp \begin{bmatrix} \underline{\beta} \\ 0 \\ \sigma \end{bmatrix} \tag{34}$$

This is a *mixed complementarity* problem, since the middle row of Eq. 34 corresponding to the bilateral constraints must be satisfied exactly, in contrast with the inequality complementarity conditions on the first and third rows. We will hereon

refer to Eq. 34 as the *standard LCP*

$$w = Mz + q \quad \perp \quad z$$

$$\text{with } M \triangleq \begin{bmatrix} \begin{bmatrix} \bar{D}^* Q_u & \Lambda[Q_u^* \underline{D}, \; Q_b^*] \\ \bar{E} & 0 \end{bmatrix} & \begin{bmatrix} \hat{F} & 0 \\ 0 & 0 \end{bmatrix} \\ \begin{bmatrix} \bar{D}^* Q_b & \bar{D}^* v^- \end{bmatrix} & \end{bmatrix} \tag{35}$$

$$z \triangleq \begin{bmatrix} \beta \\ \lambda \\ \sigma \end{bmatrix}, \; q \triangleq \begin{bmatrix} \bar{D}^* Q_u \\ \bar{Q}_b \\ 0 \end{bmatrix} \Delta_t \alpha_f + \begin{bmatrix} \bar{D}^* v^- \\ 0 \\ 0 \end{bmatrix}$$

Analogous to Eq. 31, the solution to this $n_u(n_f + 2) + n_b$ dimensional LCP can be used to propagate the system state as follows:

$$\begin{aligned} p &= Q_u^* \underline{D}\, \beta + Q_b^* \lambda \\ \dot{\theta}^+ &= \dot{\theta}^- + M^{-1} J^* p + \Delta_t \ddot{\theta}_f \end{aligned} \tag{36}$$

IV. Collision Dynamics

During elastic collisions, some, and not all, of the impact energy is lost. The *coefficient of restitution*, $\varrho(i)$ defines the fraction of the energy that is not lost after a collision. The complementarity approach to modeling elastic collisions breaks up the collision event into instantaneous *compression* and *decompression* phases [1]. During the compression phase, collision energy is stored, and during decompression, a fraction of the collision impulse is restored.

A. Compression

The collision phase is instantaneous and impulsively changes the the relative linear contact velocity from $v_c^-(i)$ to a new $v_c^+(i)$ value with a non-negative normal component. The resulting compression impulse is denoted $p_c(i)$. The mixed LCP problem for the compression phase is obtained by setting $\Delta_t = 0$ in Eq. 34 to obtain

$$\begin{bmatrix} \begin{bmatrix} \bar{D}^* Q_u & \Lambda[Q_u^* \underline{D}, \; Q_b^*] \\ \bar{Q}_b & \\ \bar{E} & 0 \end{bmatrix} & \begin{bmatrix} \hat{F} & 0 \\ 0 & 0 \\ 0 & 0 \end{bmatrix} \\ \begin{bmatrix} \bar{D}^* v^- \\ 0 \\ 0 \end{bmatrix} & \end{bmatrix} \begin{bmatrix} \beta \\ \lambda \\ \sigma \end{bmatrix} + \begin{bmatrix} \bar{D}^* v^- \\ 0 \\ 0 \end{bmatrix} \perp \begin{bmatrix} \beta \\ 0 \\ \sigma \end{bmatrix} \tag{37}$$

The LCP solution is used to instantaneously (i.e. impulsively) propagate the state for the compression phase as follows:

$$\begin{aligned} p_c &= Q_u^* \underline{D}\, \beta + Q_b^* \lambda \\ \dot{\theta}_c^+ &= \dot{\theta}^- + M^{-1} J^* p_c \end{aligned} \tag{38}$$

$$v_c^+$$

B. Decompression

The decompression phase applies a impulse of magnitude $\varrho(i)\hat{n}^*(i)p_c(i)$ for the ith contact along the normal from the impulse stored during the compression phase. An additional contact impulse ensures that the normal component of the remains non-negative. Define the ϑ decompression impulse as

$$\vartheta \triangleq \mathrm{col}\{(\varrho(i)\hat{n}^*(i)p_c(i))\,\hat{n}(i)\}_{i=1}^{n_u} \in R^{3n_u} \tag{39}$$

The decompression phase LCP has the form:

$$\begin{bmatrix} \begin{bmatrix} \bar{D}^* Q_u & \Lambda[Q_u^* \underline{D}, \; Q_b^*] \\ \bar{Q}_b & \\ \bar{E} & 0 \end{bmatrix} & \begin{bmatrix} \hat{F} & 0 \\ 0 & 0 \\ 0 & 0 \end{bmatrix} \\ \begin{bmatrix} \bar{D}^* v_c^+ & \bar{D}^* Q_u \\ 0 & Q_b \\ 0 & 0 \end{bmatrix} & \end{bmatrix} \begin{bmatrix} \beta \\ \lambda \\ \sigma \end{bmatrix} + \begin{bmatrix} \bar{D}^* v_c^+ \\ 0 \\ 0 \end{bmatrix} \perp \begin{bmatrix} \beta \\ 0 \\ \sigma \end{bmatrix} \tag{40}$$

The decompression LCP problem is the the standard LCP in Eq. 35 with $\Delta_t = 0$, the contact linear velocity v_u^- replaced with v_c^+, and an additional $\begin{bmatrix} \bar{D}^* Q_u \\ Q_b \end{bmatrix} \Lambda Q_u^* \vartheta$ term for the LCP q vector term. The LCP solution is used to instantaneously propagate the state for the decompression phase as follows:

$$\begin{aligned} p &= Q_u^* \underline{D}\, \beta + Q_b^* \lambda + Q_u^* \vartheta \\ \dot{\theta}^+ &= \dot{\theta}^c + M^{-1} J^* p \end{aligned} \tag{41}$$

For inelastic collisions, $\varrho(i) = 0$, and for this case there is no decompression phase. For collision dynamics, the numerical state propagation process consists of the following steps:

1) Use Eq. 36 to obtain new $[\theta(t + \Delta_t), \dot{\theta}(t + \Delta_t)]$ from the $[\theta(t), \dot{\theta}(t)]$ state.
2) If the new $[\theta(t + \Delta_t), \dot{\theta}(t + \Delta_t)]$ state involves a new collision, then estimate the Δ_t time for collision, and redo Step (1) with this new time interval. This should bring the system into contact for the new collision. Now use the compression and decompression LCPs in Eq. 38 and Eq. 41 to propagate the system through the collision.

V. Spatial Operator Computational Algorithm

The key implementation and computational challenge with using minimal coordinates is the need for computing the $\underline{\Lambda}$ needed for setting up and solving the LCP problems in Eq. 28, Eq. 34, Eq. 37 and Eq. 40. As seen in Eq. 6, $\underline{\Lambda}$ involves the configuration dependent matrix products of the Jacobian matrix and the mass matrix inverse. A direct evaluation of this expression would be of $O(N^3)$ computational cost. However references [3, 4, 6] have used spatial operators to develop simpler and recursive computational algorithms for $\underline{\Lambda}$ that are of only $O(N)$ complexity. We briefly sketch out below the relative linear velocity at the end of the decompression step

underlying analysis and structure of this algorithm, and refer the reader to [3, 4, 6] for more notation and derivation details.

A. Spatial operator factorization of M^{-1}

We begin with the following key spatial operator based analytical results that provide explicit, closed-form expressions

for the factorization and inversion of a tree mass matrix [4, 8]:

$$\begin{aligned} M &= H\phi M\phi^* H^* \\ M &= [I + H\phi K]\, D\, [I + H\phi K]^* \\ [I + H\phi K]^{-1} &= [I - H\psi K] \\ M^{-1} &= [I - H\psi K]^* D^{-1} [I - H\psi K] \end{aligned} \tag{42}$$

The first expression defines the Newton-Euler operator factorization of the mass matrix M in terms of the H hinge articulation, the ϕ rigid body propagation and the M link spatial inertia operators. While this factorization has non-square factors, the second expression describes an alternative factorization involving only square factors with block diagonal D and block lower-triangular $[I+H\phi K]$ matrices. This factorization involves new spatial operators that are associated with the *articulated body (AB)* forward dynamics algorithm [2, 3] for the system. The next expression describes an analytical expression for the inverse of the $[I + H\phi K]$ operator. Using this leads to the final analytical expression for the inverse of the mass matrix. These operator expressions hold generally for tree-topology systems irrespective of the number of bodies, the types of hinges, the specific topological structure and even for the case of non-rigid links [4].

B. The Ω extended operational space compliance matrix

With $V \in R^{6n}$ denoting the stacked vector of link spatial velocities, its spatial operator expression is [4]

$$V = \phi^* H^* \dot{\theta} \tag{43}$$

With O_k^i denoting the ith node on the kth link, its spatial velocity $V(O_k^i)$ can be obtained from the spatial velocity $V(k)$ of its parent link via the following rigid body transformation:

$$V(O_k^i) = \phi^*(k, O_k^i) V(k) \tag{44}$$

Bundling together these rigid body transformations for all nodes we define the $B \in R^{6n_c \times 6n}$ *pick-off* matrix such that

$$V_c = BV \overset{43}{=} B\phi^* H^* \dot{\theta} \quad \Rightarrow \quad J \overset{3}{=} B\phi^* H^* \tag{45}$$

This is the spatial operator expression for the J Jacobian matrix. Using this expression and Eq. 42 for the mass matrix inverse within Eq. 6 leads to the following expression for $\underline{\Lambda}$:

$$\begin{aligned} \underline{\Lambda} &\overset{6}{=} J M^{-1} J^* \\ &\overset{42}{=} B^* \phi^* H^* (I - H\psi K)^* D^{-1} (I - H\psi K) H\phi B \end{aligned} \tag{46}$$

Using the following spatial operator identity from [4, 8]

$$(I - H\psi K) H\phi = H\psi \tag{47}$$

in Eq. 46 leads to the following simpler expression for $\underline{\Lambda}$:

$$\Lambda = B^* \Omega B, \quad \text{where} \quad \Omega \triangleq \psi^* H^* D^{-1} H \psi \in R^{6n_c \times 6n_c} \tag{48}$$

We have arrived at an expression for $\underline{\Lambda}$, that unlike Eq. 6, involves neither the mass matrix inverse nor the node's Jacobian matrix! We refer to Ω as the *extended operational space compliance matrix*. This terminology is based on Eq. 48 which shows that the OSCM, $\underline{\Lambda}$ can be obtained by a reducing transformation of the full, all body Ω matrix by the B pick-off operator involving just the matrix sub-blocks associated with the parent links of the nodes. From its definition, it is clear that Ω is a symmetric and positive semi-definite matrix, since D^{-1} is a symmetric positive-definite matrix.

While the explicit computation of M^{-1} or J is not needed to obtain $\underline{\Lambda}$, the direct evaluation of Eq. 48 still remains of $O(N^3)$ complexity due to the need for carrying out the multiple matrix/matrix products. The next section shows that these matrix/matrix products can be avoided by exploiting a decomposition of the Ω matrix.

C. Decomposition of Ω

A following lemma describes a decomposition of Ω into simpler component terms and an expression for its block elements. The E_ψ^* and $\psi()$ terms used below are defined in references [3, 4]. Furthermore, $\wp(k)$ denotes the parent link for the kth link, and $i \prec j$ notation implies that the jth link is an ancestor of the ith link in the tree.

Lemma 1 Decomposition of Ω

Ω can be decomposed into the following disjoint sum of component terms:

$$\Omega \triangleq \Upsilon + \tilde{\psi}^* \Upsilon + \Upsilon \tilde{\psi} + R$$

$$\text{where} \quad R = \sum_{\substack{\forall i,j:\, i \not\prec\succ j \\ k = \wp(i,j)}} e_i \psi^*(k,i) \Upsilon(k) \psi(k,j) e_j^* \tag{49}$$

$\Upsilon \in R^{6n_c \times 6n_c}$ is a block-diagonal operator, referred to as the operational space compliance kernel, satisfying the following backward Lyapunov equation:

$$H^* D^{-1} H = \Upsilon - \text{diagOf}\left(E_\psi^* \Upsilon E_\psi \right) \tag{50}$$

$\text{diagOf}\left(E_\psi^* \Upsilon E_\psi \right)$ represents just the block-diagonal part of the (generally non block-diagonal) $E_\psi^* \Upsilon E_\psi$ matrix. The 6×6 dimensional, symmetric, positive semi-definite $\Upsilon(k)$ diagonal matrices satisfy the following parent/child recursive relationship:

$$\Upsilon(k) = \psi^*(\wp(k), k) \Upsilon(\wp(k)) \psi(\wp(k), k) + H^*(k) D^{-1}(k) H(k) \tag{51}$$

This relationship forms the basis for the following $O(N)$ base-to-tips scatter recursion for computing the $\Upsilon(k)$ diagonal elements:

for *all nodes* k *(base-to-tips scatter)*

$$\begin{aligned} \Upsilon(k) = {} & \psi^*(\wp(k), k) \Upsilon(\wp(k)) \psi(\wp(k), k) \\ & + H^*(k) D^{-1}(k) H(k) \end{aligned} \tag{52}$$

end loop

While Υ defines the block-diagonal elements of Ω, the following recursive expressions describe its off-diagonal terms:

$$\Omega(i,j) = \begin{cases} \Upsilon(i) & \textit{for } i = j \\ \Omega(i,k)\psi(k,j) & \textit{for } i \not\succ k > j, \quad k = \wp(j) \\ \Omega^*(j,i) & \textit{for } i < j \\ \Omega(i,k)\psi(k,j) & \textit{for } i \not\succ j,\ j \not\succ i,\ k = \wp(i,j) \end{cases} \tag{53}$$

Proof: See [3, 4]. ■

Eq. 49 shows that Ω can be decomposed into the sum of simpler terms consisting of the block diagonal Υ, the upper-triangular $\tilde{\psi}^*\Upsilon$, the lower triangular $\Upsilon\tilde{\psi}$, and the sparse R matrices. Furthermore, Eq. 53 reveals that all of the block-elements of $\Omega(i,j)$ can be obtained from the $\Upsilon(i)$ elements of the Υ block-diagonal operational space compliance kernel. Since only a small subset of the elements of Ω are needed for computing Λ, Section V-D later exploits this to avoid the expensive computation of the full Ω matrix.

D. Computing $\underline{\Lambda}$

From the $\underline{\Lambda} = B^*\Omega B$ expression, and the sparse structure of B, it is clear that only a subset of the elements of Ω are needed to compute $\underline{\Lambda}$. The B pick-off operator has one column for each of the O_k^i task space nodes, with each such column having only a single non-zero 6×6 matrix entry at the kth parent link slot. From this structure of B and Eq. 48, the 6×6 block matrix elements of the $\underline{\Lambda}$ OSCM are given by the following expression:

$$\underline{\Lambda}(O_k^i, O_j^l) = \phi^*(k, O_k^i)\Omega(k,j)\phi(j, O_j^l) \tag{54}$$

Here, O_k^i and O_j^l denote a pair of nodes on the kth and j^{th} links, respectively. It is therefore evident that only as many elements of Ω as there are elements in $\underline{\Lambda}$ are needed. Thus, just $n_c \times n_c$ number of 6×6 sub-block matrices of Ω are required. In view of the symmetry of the matrices, we need just $n_c(n_c+1)/2$ such sub-block matrices. The overall cost of this algorithm is linearly proportional to the number of degrees of freedom, and a quadratic function of the number of nodes, which is much lower than the $O(N^3)$ cost implied by Eq. 6.

E. Illustrative simulation example

To illustrate our results, we use a simulation of a multi-link pendulum colliding with itself and the environment. The environment consists of a floor centered at $z = 0$m and a wall centered at $x = 4$m. Both the floor and wall have a width of 0.2m. The multi-link pendulum itself consists of n identical bodies connected with pin hinges. The bodies are modeled as spheres with a mass of 1.0kg each. The radius of the sphere depends on the number of links present in order to maintain the general dimensions of the pendulum itself and is chosen as $3.0/n$m and the distance between each hinge is set to $6.0/n$m. The pendulum base is situated at a height of 10.0m.

.

The simulation lasts for 5 seconds with a time step of 1ms. The coefficient of restitution was set to 0 to simulate an inelastic system. The pendulum starts raised to an angle of $\pi/2$ radians with an initial angular velocity of -1 radians/s and a standard gravitational acceleration of 9.8m/s^2.

As seen in Figure 1, as the 15-link pendulum swings from left to right, it collides with the ground, drags along the ground, and eventually collides with the wall on the right. In the course of the sequence, multiple links are at times in collision with the ground, the wall and with each other.

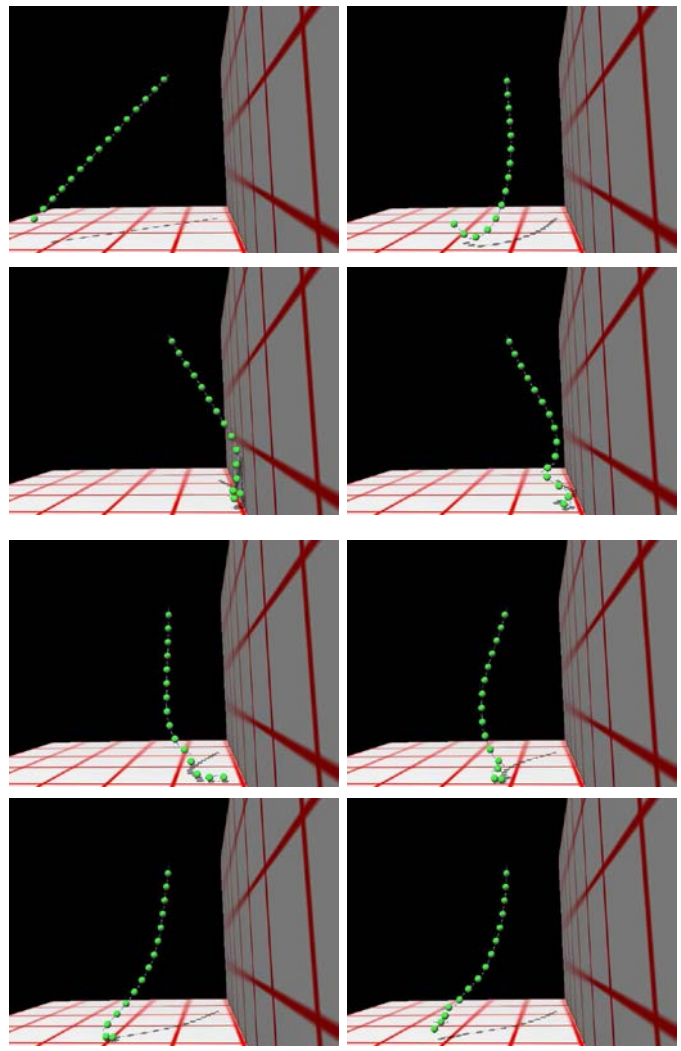

Fig. 1. Time series capture of swinging pendulum simulation with 15 links

We simulate the contact and collision dynamics using two different techniques. In the first *tree-augmented (TA)* technique, the serial-chain pendulum is modeled with minimal coordinates and only unilateral contact constraints. The second *fully-augmented (FA)* technique uses redundant coordinates where each link is treated as an independent body, and the hinges are handled as bilateral constraints between the neighboring links. We have verified good agreement between the solutions from these two methods, Figure 2 shows the similar time history of the height of the last link of a 3-body pendulum from the two methods.

Table I compares the computational cost of the TA and FA methods for pendulums containing 3 to 30 links. We

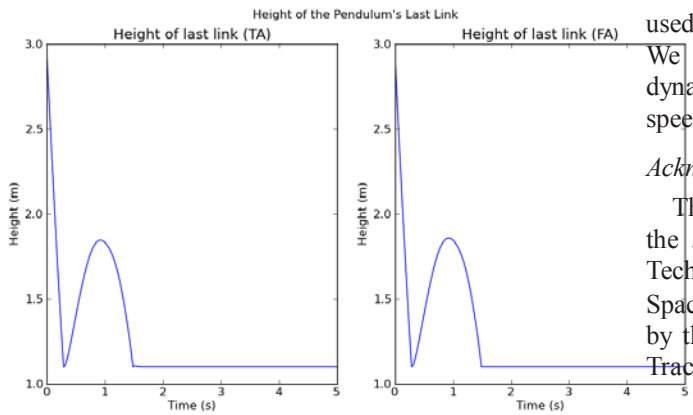

Fig. 2. Comparison of the height of the last link using Tree Augmented and Fully Augmented methods for a 3-body pendulum

	Computation Time (s)	
Number of Bodies	Tree Augmented	Fully Augmented
3	1.326214	5.035574
6	1.572062	7.585271
12	3.231113	21.002845
15	2.930593	40.110204
24	5.989333	117.906592
30	4.766953	212.037019

TABLE I
A COMPARISON OF THE COMPUTATIONAL TIME FOR THE MINIMAL COORDINATE TA AND THE NON-MINIMAL FA COORDINATE TECHNIQUES FOR THE MULTI-LINK PENDULUM EXAMPLE WITH DIFFERENT NUMBER OF LINKS.

observe that the redundant coordinates FA method is 3 to 40 times computationally more expensive than the minimal coordinates TA method. Moreover the performance gap widens substantially as the number of links in the system is increased.

VI. CONCLUSIONS

In this article we have described the formulation of the contact and collision dynamics for multi-link systems using minimal coordinates. With minimal coordinates, the size of the standard LCP problem in Eq. 35 is $n_u(n_f + 2) + n_b$ which is independent of the number of links or the number of degrees of freedom in the system. In contrast, the size of the corresponding LCP problem using redundant coordinates would have dimension larger by $6n - N$ or more depending on the specific formulation. For a 6-link manipulator with 6 degrees of freedom, this would amount to dimensional increase of 30. The use of minimal coordinates also results in the automatic enforcement of the bilateral constraints such as from inter-link hinges and avoids the need for DAE type error control schemes for inter-link hinge bilateral constraints. We have described the variants of the LCP problem needed to handle effects such as bilateral constraints associated with closed-chain topologies as well as elastic and inelastic collision dynamics. Finally, we have shown that existing low order computational algorithms for computing the OSCM can be used to make the computation of the LCP matrices tractable. We have used a multi-link pendulum contact and collision dynamics simulation example to illustrate the computational speedup achieved by the minimal coordinate approach.

Acknowledgments

The research described in this paper was performed at the Jet Propulsion Laboratory (JPL), California Institute of Technology, under contract with the National Aeronautics and Space Administration.[4] This project was also supported in part by the DARPA Autonomous Robotic Manipulation Software Track (ARM-S) program.

REFERENCES

[1] M Anitescu and F A Potra. Formulating dynamic multi-rigid-body contact problems with friction as solvable linear complementarity problems. Nonlinear Dynamics, 14(3):231–247, 1997. ISSN 0924090X. doi: 10.1023/A:1008292328909.

[2] Roy Featherstone. Rigid Body Dynamics Algorithms. Springer Verlag, 2008.

[3] Abhinandan Jain. Graph Theoretic Foundations of Multibody Dynamics Part II: Analysis and Algorithms. Multibody System Dynamics, 26(3):335–365, October 2011. ISSN 1384-5640. doi: 10.1007/s11044-011-9267-6.

[4] Abhinandan Jain. Robot and Multibody Dynamics: Analysis and Algorithms. Springer, 2011. ISBN 1441972668. doi: 10.1007/978-1-4419-7267-5.

[5] Oussama Khatib. A Unified Approach for Motion and Force Control of Robot Manipulators: The Operational Space Formulation. IEEE Journal of Robotics and Automation, RA-3(1):43–53, February 1987.

[6] K Kreutz-Delgado, Abhinandan Jain, and Guillermo Rodriguez. Recursive formulation of operational space control. The International Journal of Robotics Research, 11(4):320–328, 1992.

[7] F Pfeiffer. Mechanical System Dynamics. Springer, 2005.

[8] Guillermo Rodriguez, Abhinandan Jain, and K Kreutz-Delgado. A spatial operator algebra for manipulator modeling and control. The International Journal of Robotics Research, 10(4):371, 1991.

[9] D. Stewart and Jeffrey C Trinkle. An implicit time-stepping scheme for rigid body dynamics with Coulomb friction. In Proceedings 2000 ICRA. Millennium Conference. IEEE International Conference on Robotics and Automation. Symposia Proceedings (Cat. No.00CH37065), pages 162–169. Ieee, 2000. ISBN 0780358864. doi: 10.1109/ROBOT.2000.844054.

[10] A Tasora, D Negrut, and M Anitescu. Large-Scale Parallel Multibody Dynamics with Frictional Contact on the Graphical Processing Unit. Journal of Multi-Body System Dynamics, 222(K4):315–326, 2008.

[4] © 2012 California Institute of Technology. Government sponsorship acknowledged.

[11] Jeffrey C Trinkle. Formulation of Multibody Dynamics as Complementarity Problems. In ASME International Design Engineering Technical Conference, Chicago, IL, September 2003.

[12] Katsu Yamane and Yoshihiko Nakamura. A Numerically Robust LCP Solver for Simulating Articulated Rigid Bodies in Contact. In Robotics: Science and Systems IV, chapter A numerica, pages 89–104. MIT Press, 2009. ISBN 0262513099.